AGU PUBLICATIONS

Geophysical Research Letters

RESEARCH LETTER
10.1002/2015GL067038

Key Points:
- Explore the turbulent mixing caused by trapped diurnal tides on deep coral mounds
- Turbulent mixing efficiently redistributes oxygen, and possibly nutrients, in the water column
- Establish a link between mixing, nutrient availability, and cold-water coral mound growth

Correspondence to:
F. Cyr,
frederic.cyr@nioz.nl

Citation:
Cyr, F., H. van Haren, F. Mienis, G. Duineveld, and D. Bourgault (2016), On the influence of cold-water coral mound size on flow hydrodynamics, and vice versa, *Geophys. Res. Lett.*, *43*, 775–783, doi:10.1002/2015GL067038.

Received 15 NOV 2015
Accepted 2 JAN 2016
Accepted article online 8 JAN 2016
Published online 30 JAN 2016

On the influence of cold-water coral mound size on flow hydrodynamics, and vice versa

Frédéric Cyr[1], Hans van Haren[1], Furu Mienis[1], Gerard Duineveld[1], and Daniel Bourgault[2]

[1]Royal Netherlands Institute for Sea Research (NIOZ), Den Burg, Netherlands, [2]Institut des Sciences de la Mer de Rimouski, Université du Québec à Rimouski, Rimouski, Québec, Canada

Abstract Using a combination of in situ observations and idealistic 2-D nonhydrostatic numerical simulations, the relation between cold-water coral (CWC) mound size and hydrodynamics is explored for the Rockall Bank area in the North Atlantic Ocean. It is shown that currents generated by topographically trapped tidal waves in this area cause large isopycnal depressions resulting from an internal hydraulic control above CWC mounds. The oxygen concentration distribution is used as a tracer to visualize the flow behavior and the turbulent mixing above the mounds. By comparing two CWC mounds of different sizes and located close to each other, it is shown that the resulting mixing is highly dependent on the size of the mound. The effects of the hydraulic control for mixing, nutrient availability, and ecosystem functioning are also discussed.

1. Introduction

Cold-water coral (CWC) reefs are known for hosting complex and rich ecosystems [*Henry and Roberts*, 2007; *Roberts et al.*, 2008]. Because CWC are essentially filter feeders, their distribution, shape, and growth are intimately linked to particle and nutrient fluxes found in regions influenced by strong currents or turbulent mixing. For example, the presence of CWC was associated to flow acceleration over topography [*Genin et al.*, 1986; *Duineveld et al.*, 2007; *Davies et al.*, 2009; *Rüggeberg et al.*, 2011] or to internal wave mixing [*Frederiksen et al.*, 1992; *White et al.*, 2005; *van Haren et al.*, 2014]. However, the exact causal relationship between CWC reef development and the hydrodynamics is still an open question. Addressing this question is challenging, especially considering that by forming reefs or mounds, CWC can modify their own hydrodynamical environment. Using a combination of in situ observations and idealized numerical simulations, the relationship between the size of CWC mounds and the local hydrodynamics is explored.

The focus is on the northwest European shelf, known for hosting several CWC mound clusters (or provinces) along the continental slopes [*Roberts et al.*, 2008; *White and Dorschel*, 2010]. Geological evidence exists of successive mound growth in the area over the past 2.6 Ma [*Thierens et al.*, 2010]. From a physical point of view, this region is also known for its "extraordinary" tidal currents [*Moray*, 1665; *Cartwright*, 1969] resulting from the diurnal tidal waves being trapped and driven to resonance by the topographical features [*Longuet-Higgins*, 1968; *Huthnance*, 1974; *Pingree and Griffiths*, 1984]. This enhancement of the barotropic current velocities is particularly important above the eastern slope of Rockall Bank (Figure 1). These trapped waves may be visualized as alternating cyclonic/anticyclonic eddy-like cells moving southwest along the bank edge (see alternate red and blue cells of Figure 1). The translation of these cells is such that a fixed station along the slope will mainly experience a diurnal current periodicity (e.g., currents observed with 12 h delay in the red boxes of Figure 1 have opposite signs).

A recent mooring deployment above the SE Rockall Bank slope confirmed the diurnal nature of near-bottom currents in the area [*van Haren et al.*, 2014; *Cyr and van Haren*, 2015]. These studies also revealed large vertical excursions of the isopycnals (>100 m) and relatively strong diurnal currents ($|u| < 0.25$ ms^{-1}) associated with a diurnal succession of sharp temperature fronts generating high turbulence levels, with potential positive effects on exchange of particulate and dissolved compounds (e.g., oxygen and nutrients). It is therefore conjectured that strong near-bottom currents caused by the trapped waves are intimately linked with CWC growth and shapes in this area [*White et al.*, 2007; *Mienis et al.*, 2007; *van Haren et al.*, 2014].

In this area, numerous carbonate mounds of varying sizes were found with some of more than 300 m height next to mounds of ~100 m [*Mienis et al.*, 2006]. These observations thus raise questions concerning CWC

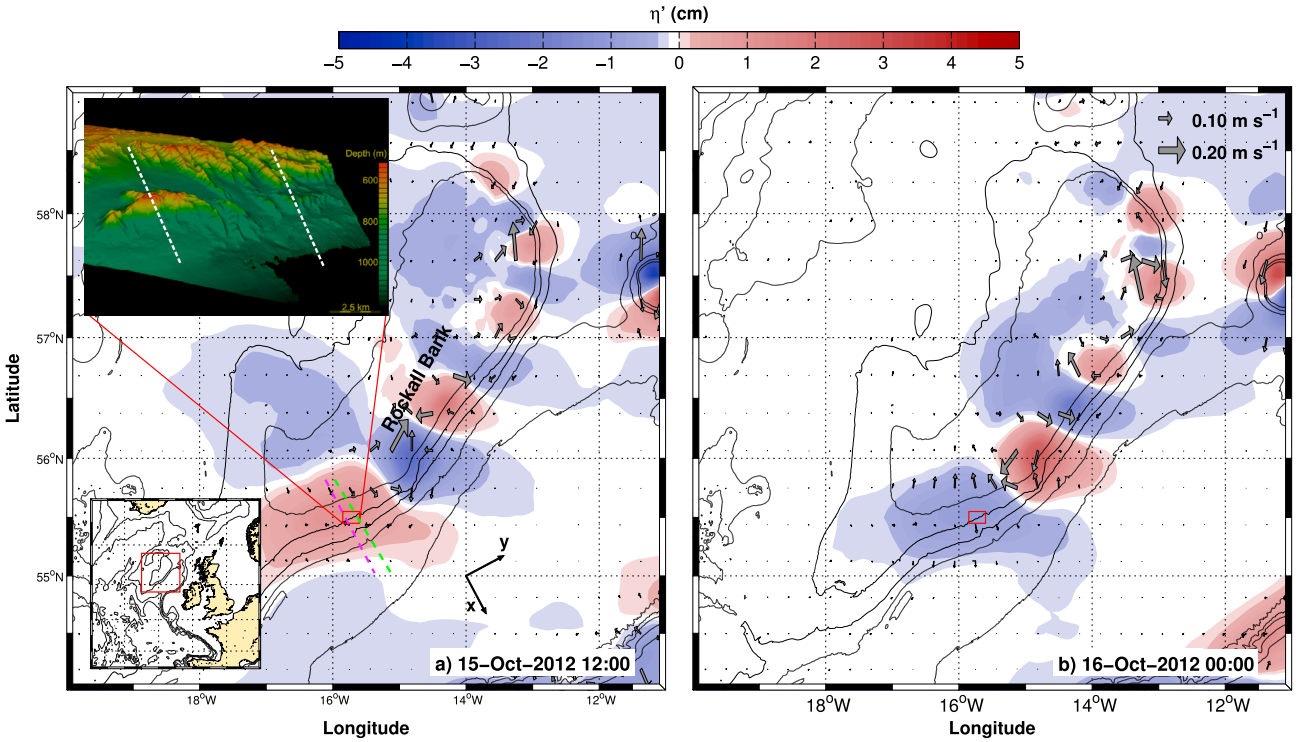

Figure 1. Bathymetry of the study area and surface tidal currents snapshots during the survey. (a) Rockall Bank (main figure), located about 400 km northwest of Ireland in the North Atlantic (lower inset). The focus is made on the Logachev CWC mounds province (upper inset, multibeam mapping) on the southern slopes of Rockall Bank. Approximate conductivity-temperature-depth (CTD) transects (white dashed lines) are drawn for reference. The model 2-D domain (magenta and green dashed lines) follows the CTD transects and are oriented according to the Cartesian axes system on the lower right. The main figure highlights sea surface anomalies η' in color (difference between local sea surface elevation and the mean elevation of the 1°×1° region around it) for 15 October, 12:00. Barotropic currents for the same period are also drawn as arrows showing current intensification at the slopes. These data (FES2012) were produced by Noveltis, Legos, and Collecte Localisation Satellites Space Oceanography division and distributed by Aviso, with support from Centre National d'Etudes Spatiales (http://www.aviso.altimetry.fr/). (b) Same data as in Figure 1a but 12 h later. The region of interest (red rectangle) is drawn in both panels for reference.

growth rates, in possible relation to different turbulence levels. This is because the strong variability of physico-chemical conditions due to mixing on the Rockall mounds would, according to *Findlay et al.* [2014], be beneficiary for the corals as it induces physiological flexibility. By comparing two coral mounds of different sizes that are separated by less than 10 km, the primary goal of this study is to highlight the different flow hydrodynamics in relation to CWC mounds sizes. Potential effects of the hydrodynamics for the redistribution of oxygen and nutrients are also explored, together with the effects for CWC ecosystems functioning and, indirectly, reef formation.

2. Methodology

2.1. In Situ Data

The data set used in this study was collected during the months of October 2012 and October 2013 during two surveys aboard the R/V *Pelagia* that aimed to characterize environmental constraints on CWC reef and mound development on the SE slopes of Rockall Bank (Figure 1). More specifically, two CWC mounds from the Logachev province are under the scope of our study. The first structure is the Haas mound, a >300 m high and ~1.5 km wide (in the cross-isobath direction) structure that emerges from the bank (see cross-isobath section in Figure 2a). This mound locally increases the slope of the bank from ~3% (between 450 and 2400 m) to ~35% on the downslope side of the CWC mound (the depth increases from 560 to 900 m over 1 km). During the 2012 survey, six conductivity-temperature-depth (CTD) transects were realized over the slope across the Haas CWC mound during a period of ~28 h.

The second structure is located less than 10 km northeast of the Haas mound, following approximately the same isobaths (see Figure 2b). This mound is smaller than the Haas mound, and its slope is slightly gentler at about 25% (the depth increases from about 790 to 975 m over 800 m). During the 2013 campaign, five CTD

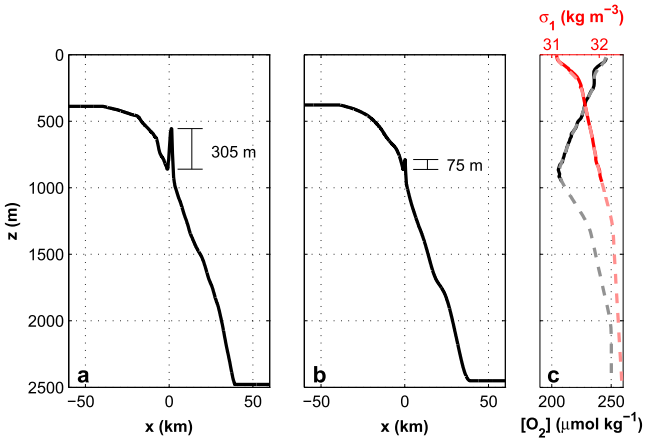

Figure 2. Numerical simulation configurations. (a) Idealized topography over the Haas CWC mound (magenta dashed line in Figure 1a). (b) Idealized topography over the smaller CWC mound (green dashed line in Figure 1a). Both topographies are built from the 30arcsec intervals General Bathymetric Chart of the Oceans (GEBCO_08 Grid, version 20100927, http://www.gebco.net) but with local refinement obtained from multibeam mapping (upper inset of Figure 1a). The domains are clipped at their minimum and maximum depths and extended at these constant depths until the boundaries located at $\pm 5 \times 10^5$ km (not shown). (c) Idealistic density (red dashed line) and oxygen concentration (gray dashed line) profiles, calculated from mean profiles obtained during the 2012 CTD transect in the 0–955 m depth range (solid lines). In the 955–1250 m depth range, these profiles match one cast realized in the deepest part of the slope during the 2013 campaign. Below 1250 m, profiles are extended to match the average of 15 Bio-Argo casts realized between January and June 2013 within a box of latitude (54–56°N) and longitude (12–18°W) encompassing our region of interest (data downloaded on 13 May 2015 at https://www.nodc.noaa.gov/argo). These data were collected and made freely available by the International Argo Program and the national programs that contribute to it (http://www.argo.ucsd.edu, http://argo.jcommops.org). The Argo Program is part of the Global Ocean Observing System. Since no climatology is available below 2000 m, these profiles are extrapolated to a constant stratification and a constant oxygen concentration in the 2000–2500 m range, respectively.

transects were realized across this mound during a period of ~21 h. During both surveys, a Seabird SBE-43 oxygen sensor was also mounted on the CTD. Oxygen concentration is used here as a conservative tracer to visualize the flow interaction with the mounds. The R/V *Pelagia* was also equipped with a Kongsberg-Simrad EM300 multibeam echosounder to map the sloping bottom in greater detail (see upper inset in Figure 1a).

Of the six CTD transects realized above the Haas mound, three are presented in Figures 3a, 3c, and 3e. This figure shows the density (black lines) and oxygen concentration (color scale) distributions, together with the topography (gray shade). These transects were composed of seven fixed CTD stations (vertical dashed lines), and each transect was completed in about 5 h. The three transects displayed here are chosen to represent the upslope flow (Figure 3a), the downslope flow (Figure 3e), and the flow reversal in between (Figure 3c). Figures 4a, 4c, and 4e show similar CTD transect data but over the smaller CWC mound.

2.2. Idealized Simulations

In order to better interpret our observations, we performed idealized numerical simulations using a two-dimensional, nonhydrostatic and fully nonlinear model initially developed by *Bourgault and Kelley* [2004] that has been modified here to include the Coriolis force. The modified version is still two-dimensional by resolving spatial gradients only in the *x*-*z* plane, but the model now incorporates an equation for an infinitely uniform velocity in the *y* direction (see axes system in Figure 1). We refer to related papers for specific details about the numerical algorithm [*Bourgault and Kelley*, 2004; *Bourgault et al.*, 2014], and only a few relevant aspects of the simulations are provided here.

The numerical domains correspond to portions of the SE slope of the Rockall Bank (Figures 2a and 2b) along two transects (respectively, magenta and green lines in Figure 1). While we use realistic topography for the slope region, the upper and lower portions of the slope outside the region of interest are clipped at the maximum and minimum depth values, respectively, and extended to $x = \pm 5 \times 10^5$ km to avoid contamination from the model boundaries (model boundaries are not shown in Figure 2).

The initial density and oxygen concentration distributions are horizontally uniform across the domain and correspond to the vertical profile presented in Figure 2c. These profiles are synthetic, as they are a mixture

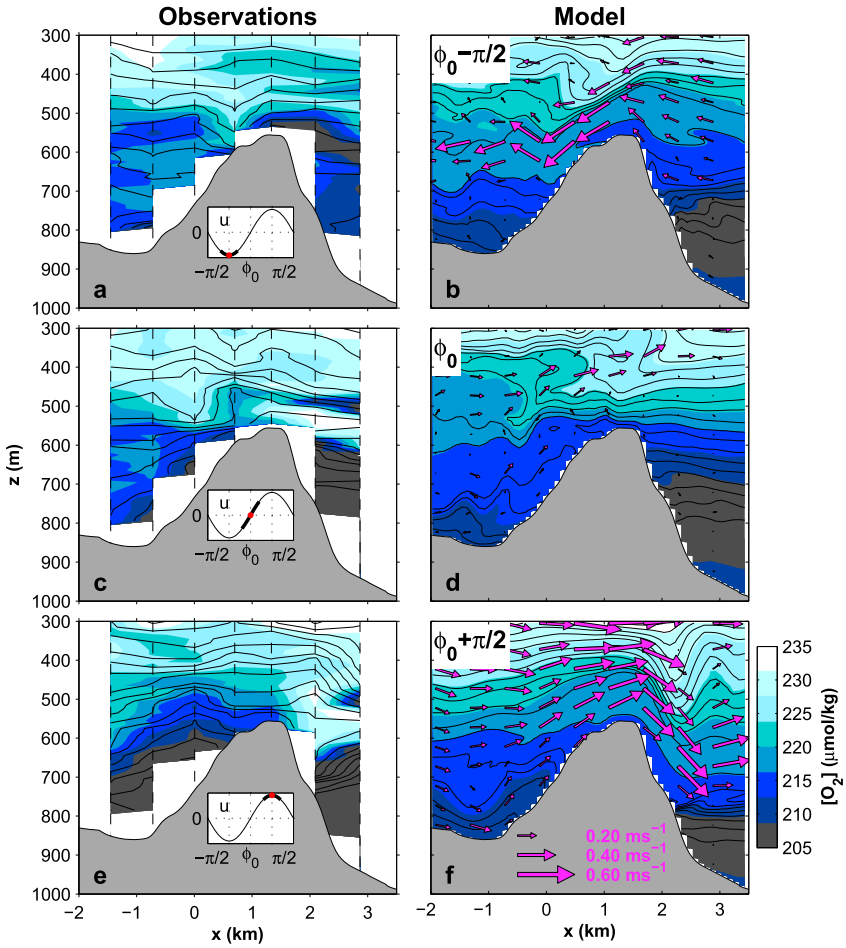

Figure 3. Observations from CTD transects and numerical simulation results across the Haas CWC mound. (a, c, e) The linearly interpolated oxygen (color) and density (solid lines) fields over seven CTD stations (vertical dashed lines). Isopycnals are separated by 0.02 kg m^{-3} intervals. The timing (start to end in UTC time) of each CTD transect is as follows: from 16 October 2012 at 20:43 to 17 October 2012 at 01:05 (Figure 3a); on 17 October 2012 from 01:05 to 06:22 (Figure 3c); and on 17 October 2012 from 06:22 to 10:52 (Figure 3e). The maximum upslope displacements is found in Figure 3c. (b, d, f) Numerical results of the same quantities, where velocity vectors above the CWC mound are drawn in purple. Note that the panels are vertically stretched, meaning that the arrow angles do not represent the true angle of the currents. The phases of these snapshots relative to the phases of the nearest current reversal are identified in the upper left corner (here $\phi = \phi_0$ corresponds to 4 days and 15 h after the beginning of the simulation). These approximately fit the timing of the corresponding transects, with the maximum upslope velocities in Figure 3b, the maximum downslope velocities in Figure 3f, and the reversal in Figure 3d. Sketches representing the phase of the measurements (thick lines) and the phase of the model results (red dots) versus cross-isobath velocities u are given in Figures 3a, 3c, and 3e.

of several sets of observations (details in Figure 2 caption). Oxygen is treated as a passive and conservative tracer in the model. It is therefore transported and modified by the same advective and diffusive processes as those applied to the density field, without any sources or sinks. The fluid is initially at rest, and the only forcing terms, F_x and F_y, are horizontally uniform barotropic pressure gradients that aim to mimic the diurnal tides present in the region. The set of equations to be resolved is thus [see also *Bourgault et al.*, 2014]

$$\frac{\partial u}{\partial t} + \frac{\partial u^2}{\partial x} + \frac{\partial (wu)}{\partial z} - fv = F_x - \frac{1}{\rho_0}\frac{\partial p}{\partial x} + \frac{\partial}{\partial x}\left(\nu_h \frac{\partial u}{\partial x}\right) + \frac{\partial}{\partial z}\left(\nu_v \frac{\partial u}{\partial z}\right), \tag{1}$$

$$\frac{\partial v}{\partial t} + \frac{\partial (uv)}{\partial x} + \frac{\partial (wv)}{\partial z} + fu = F_y + \frac{\partial}{\partial x}\left(\nu_h \frac{\partial v}{\partial x}\right) + \frac{\partial}{\partial z}\left(\nu_v \frac{\partial v}{\partial z}\right), \tag{2}$$

$$\frac{\partial w}{\partial t} + \frac{\partial (uw)}{\partial x} + \frac{\partial w^2}{\partial z} = -\frac{1}{\rho_0}\frac{\partial p}{\partial z} + \frac{\rho}{\rho_0} g + \frac{\partial}{\partial x}\left(\nu_h \frac{\partial w}{\partial x}\right) + \frac{\partial}{\partial z}\left(\nu_v \frac{\partial w}{\partial z}\right), \tag{3}$$

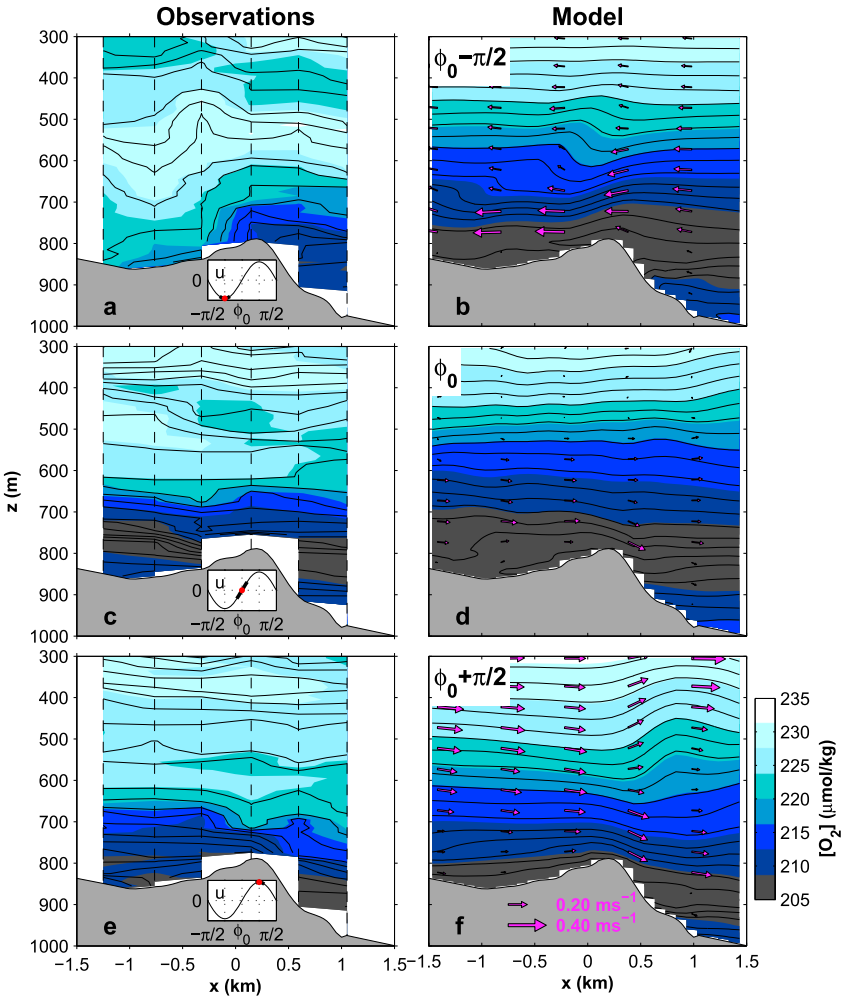

Figure 4. Same as Figure 3 but for the smaller CWC mound northeast of Haas mound. The timing of each CTD transect is as follows: (a) on 10 October 2013 from 17:47 to 21:10; (c) on 11 October 2013 from 02:27 to 05:54; and (e) on 11 October 2013 from 06:51 to 10:17.

$$\frac{\partial u}{\partial x}+\frac{\partial w}{\partial z}=0, \tag{4}$$

$$\frac{\partial \rho}{\partial t}+\frac{\partial (u\rho)}{\partial x}+\frac{\partial (w\rho)}{\partial z}=\frac{\partial}{\partial x}\left(\kappa_h\frac{\partial \rho}{\partial x}\right)+\frac{\partial}{\partial z}\left(\kappa_v\frac{\partial \rho}{\partial z}\right), \tag{5}$$

where t is time; x and z are, respectively, the across-channel and vertical axes (positive downward); u, v, and w are, respectively, the velocities along the x, y, and z axes; f is the Coriolis parameter; ρ is the water density; ρ_0 is a reference density; p is the pressure; ν_h and ν_v are the horizontal and vertical eddy viscosity, respectively; and κ_h and κ_v are the horizontal and vertical eddy diffusivity, respectively. Eddy viscosities are parametrized using the *Smagorinsky* [1963] scheme described in *Bourgault and Kelley* [2004], e.g.,

$$\nu_h=\begin{cases}(C_s\Delta x)^2\sqrt{2S^2-N^2} & \text{for } 2S^2>N^2\\ 10^{-6}\text{m}^2\text{s}^{-1} & \text{otherwise,}\end{cases} \tag{6}$$

where Δx is the horizontal grid size, $C_s=0.1$ the Smagorinsky coefficient, $N^2=(g/\rho_0)\partial\rho/\partial z$ the buoyancy frequency squared, and S^2 is the square of the strain rate tensor as detailed in the appendix in *Bourgault and Kelley* [2004] but with the addition of terms to take into account the strain rate caused by the gradients of v (e.g., $\partial v/\partial x$ and $\partial v/\partial z$). Similar expressions are used for the eddy diffusivities except that minimum values are set to 10^{-7} m^2 s^{-1} for $2S^2<N^2$. Note that we used variable horizontal and vertical grid cell sizes, with refinement around the CWC mounds ($\Delta_{x_{\min}}=100$ m, $\Delta_{x_{\max}}=5\times10^6$ m, $\Delta_{z_{\min}}=2.5$ m, and $\Delta_{z_{\max}}=50$ m).

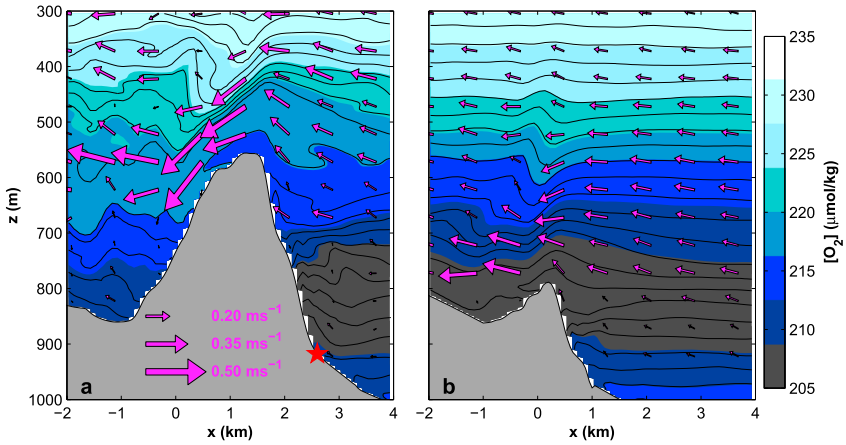

Figure 5. Comparison between the numerical simulations after 4 days and 15 h. (a) Haas CWC mound (zoom from Figure 3b). (b) Smaller CWC mound located 10 km north of Haas mound (zoom from Figure 4b). Oxygen (color), density (solid lines), and velocities (arrows) are shown. The red star is the location of the mooring described in *van Haren et al.* [2014].

In equations (1) and (2), the forcing terms are $F_x = g\frac{\partial \eta'}{\partial x}\sin(\omega t - 2\pi/3)$ and $F_y = g\frac{\partial \eta'}{\partial y}\sin(\omega t)$, with $\omega = 2\pi/86400$ rad s^{-1} the diurnal frequency and $\frac{\partial \eta'}{\partial x} = 5 \times 10^{-7}$ and $\frac{\partial \eta'}{\partial y} = 7.5 \times 10^{-7}$ the approximated slope of the surface deformation calculated from one month (October 2010) of sea surface elevation anomaly (e.g., η' in Figure 1). This can be visually understood from Figure 1 where cells having $\Delta\eta' \simeq 0.05$ m elevation and length scales of about $\Delta x \simeq 100$ km in x and $\Delta y \simeq 65$ km in y are found near the study region. The phase lag $-2\pi/3$ in F_x was set to adjust the phase differences between u and v to those observed by *van Haren et al.* [2014]. Comparison between modeled and observed near-bottom currents at the base of the Haas mound (from *van Haren et al.* [2014]; see red star in Figure 5 for mooring location) shows that the model captures 56% of the current variance in v and 24% in u, when computed in the 820–900 m depth range, i.e., where velocity measurements are available. The relatively low variance percentage resolved for this depth range, specially for u, is due to the presence the strong nonlinear bores described in *Cyr and van Haren* [2015] that the model is unable to reproduce (not shown).

3. Results

CTD transect observations and numerical results are analyzed for both CWC mounds in Figures 3 and 4. A sketch representing the exact model phase and the approximate phase of the CTD transects accompany each panel (sinusoidal plot overlay in the topography in Figures 3a, 3c, 3e, 4a, 4c, and 4e). Note that snapshots from the fifth diurnal tidal cycle of the simulations are presented here (see Figure 3 caption), but each tidal cycle exhibit similar behavior, although with some changes from one cycle to another due to the distortion of the density and velocity fields caused by the interaction of the flow with the mound.

For the Haas mound (Figure 3), the numerical results exhibit qualitative resemblances with the observations. Notable features include vertical isopycnal displacements of more than 100 m, both in the observations and in the simulation, likely caused by the interaction of the flow with the coral mound. These occur during the periods of maximum upslope and downslope velocities above the mound (respectively, Figures 3a and 3b and Figures 3e and 3f), when a depression of the isopycnals occurs on the lee side of the flow (left of the mound in Figure 3b and right in Figure 3f), suggesting hydraulic control of the flow. At the maximum upslope displacements, isopycnals plunge down on the left side of the CWC, both in the observations and in the model (Figures 3c and 3d). Vertical inversions in the oxygen field also suggest that turbulent mixing is at work above the mound. The most important of these inversions occur during the reversal of the tidal currents (Figure 3c) and is seen as a ~50 m thick layer of oxygenated waters (concentration increase from about 205 to 235 μmol kg^{-1}) injected between 500 and 600 m for $x > 1$ km. This high oxygen anomaly extends to at least 2–3 km in the x direction. Low oxygen anomalies for the same depth range are also found in Figure 3a, likely resulting from mixing at the top of the mound. The shear present during the current reversal (suggested by the numerical simulation, Figure 3d over the mound) may be responsible for the inversion of oxygen by

overturning motions. While this oxygen anomaly remains in the observations after the cross-isobath flow reversal (Figure 3e), it has disappeared in the simulation (Figure 3f). Numerical diffusion may be responsible for the rapid mixing of this tracer in the model.

Another hydrodynamic aspect is that the isopycnals located deeper than 600 m on the downslope side of the mound do not clearly rise above the summit of the mound during any tidal phase (both in observations and in the simulation). They rather plunge down when pushed against the mound (see the deepest isopycnals in Figures 3a and 3b), suggesting a blocking of the flow. This is also visible in Figures 3c and 3d, where the oxygen-poor layer (dark gray) is blocked on the right side of the mound (note that the dark gray layer found on the left side of the mound in Figure 3e likely comes from the water flowing from the sides of the mound later in the tidal cycle, not from above it). Since the oxygen minimum layer east of Rockall Bank marks the bottom of the nutrient-depleted layer (this can be seen in *McGrath et al.* [2012, Figures 5b, 6a, and 6b]), it also means that the top of the Haas mound is not regularly washed by nutrient-rich waters from below.

For the smaller CWC mound (Figure 4), the hydraulic control of the flow is different. Except for Figure 4a, isopycnal depressions on the lee side are present but weaker than in Figure 3. The simulation also shows less overturning than for the Haas mound, although density inversions in Figures 4b and 4d suggest some mixing close to the top of the mound. This mound also does not clearly block the flow, and the incoming oxygen-depleted waters from below the summit are able to flow over it, both in the observations and in the simulation. This means that this smaller CWC mound is periodically washed by deep nutrient-rich waters at a diurnal frequency. Below about 700 m, the observed sloshing motion of deep water flowing up and down the mound shows qualitative similarities with the model results. However, the large isopycnals heaving in Figure 4a is not reproduced by the model and therefore may not be due to the interaction of the barotropic tidal flow with this CWC mound. One explanation for these observed vertical excursions is that they may be due to the interaction of the flow with the 3-D topography which cannot be captured by the 2-D model. Indeed, for this phase, the barotropic flow first meets the Haas mound before meeting the smaller mound northeast of it (see upper inset in Figure 1). Trapped internal tides generated by the interaction of the barotropic flow with the topography may also explain these vertical isopycnal motions.

4. Discussion and Conclusion

4.1. Model Limitations

Unlike recent 3-D numerical work on CWC ecosystems [*Henry et al.*, 2013; *Moreno Navas et al.*, 2014], or more specifically on Rockall Bank [*Mohn et al.*, 2014], our approach here is to use an idealistic 2-D model in order to focus on one specific mechanism: cross-isobath motions and internal wave generation by topographically trapped waves. This process-based approach allows us to perform relatively inexpensive nonhydrostatic numerical simulations, preferable in this case due to the highly nonlinear internal bores and rapid density perturbations seen in the observations [*van Haren et al.*, 2014; *Cyr and van Haren*, 2015]. This approach may be justified by the relative symmetry of the Rockall Bank slope and the small size of trapped waves compared to the size of the bank (Figure 1). The present model, however, produces satisfying results for the purpose of this study, especially in terms of reproducing the characteristics of the water column observed during two transect surveys above two CWC mounds. It suggests that the modulation of currents and turbulence are primarily caused by the trapped diurnal tidal wave, thereby discrediting the potential role of critical reflection of freely propagating internal waves as main drivers explaining the presence of CWC in this area (for a discussion on the role of freely propagating internal tides for CWC see, for example, *White and Dorschel* [2010] and *Mohn et al.* [2014]). This model, however, falls short in representing the along-isobath residual circulation, hypothesized by *Mohn et al.* [2014] to retain fresh organic material in close proximity of the Rockall slopes. Although not under the scope if this study, it is worth noting that the model is also unable to reproduce the energetic bore propagation observed at the base of the Haas mound [*Cyr and van Haren*, 2015].

4.2. Influence of CWC Mound Size on the Hydrodynamics

The different flow behavior between the two mounds is summarized in Figure 5. It can be seen that the Haas mound induces a stronger hydraulic control on the flow compared to the smaller CWC mound. The parameter space that describes this periodic flow is difficult to establish for two reasons: (1) the ridge is not isolated but rather consists of a bump on a slope; and (2) the frequency of the flow is diurnal, such that the slope cannot be characterized as being subcritical/supercritical because the internal waves are trapped (no tidal rays can

escape from the slope). In this regard, the flow is better described by an analogy with steady flows because the tidal excursion distance is larger than the width of the obstacle $\left(\frac{2\pi U_0}{\omega L} > 1\right)$, where $U_0 \sim 10^{-1}$ ms^{-1}, an order of magnitude for the modeled velocity far from the topography, and $L \sim 10^3$ m an order of magnitude for the width of the mounds. In steady flows, or in this case when the flow is affected by the full topographic height of the mound, the topographic Froude number better describes the obstruction of the flow by the topography, $Fr = \frac{U_0}{Nh_0}$, where h_0 is the topography height and N the buoyancy frequency [*Legg and Klymak*, 2008]. For $Fr \ll 1$, strongly nonlinear lee waves are generally expected to occur [*Legg and Klymak*, 2008; *Klymak et al.*, 2010].

For the two numerical simulations presented here, only the parameter h_0 is varied, with $h_0 = 305$ m for the Haas mound and $h_0 = 75$ m for the smaller CWC mound (Figures 2a and 2b). Using $N \simeq 2 \times 10^{-3}$ s^{-1}, the mean buoyancy frequency calculated from the density profile of Figure 2c between 250 and 1000 m, we find $Fr \sim 10^{-1} \ll 1$ and $Fr \sim 1$ for the Haas mound and the smaller CWC mound, respectively. These calculations are in line with those depicted in Figure 5, i.e., a strong blocking with nonlinear lee wave/hydraulic jump generation for the Haas mound and a weaker blocking for the smaller mound. Given the acceleration of the flow above the higher mound to about $U = 0.35$ ms^{-1} (Figure 5b), the vertical excursion of the isopycnals associated with the hydraulic jump may be predicted to be $\Delta z = \frac{U}{N} \simeq 175$ m [*Legg and Klymak*, 2008], i.e., in line with in situ observations and model results (Figure 3).

This also indicates that when the tidal flow relaxes, the lee wave should evolve in an upstream-propagating (toward the summit) bore-like structure with considerable implication for mixing [*Legg and Klymak*, 2008; *Klymak et al.*, 2010]. The latter is also suggested by the numerical results, where an overturning structure (just left of the summit in Figure 3d) remnant of the lee wave of Figure 3b is swept on the top of the mound. Steep isopycnals just left of the summit in Figure 3c may also suggest such behavior in the observations. It is likely that the mixing energy released during this flow reversal is responsible for the oxygen input in depth (and possible nutrient redistribution) observed in observations (Figures 3c and 3e, 500–600 m, right of the mound summit). Such bore-like structures were observed by *van Haren et al.* [2014] and *Cyr and van Haren* [2015] at the base of the Haas mound between about 800 and 900 m (red star in Figure 5b). However, these structures are likely not generated by the same mechanism since the mooring was deployed in the region where the flow is blocked and in a depth range deeper than what the hydraulic jump can reach (maximum depth is $\Delta z \simeq 175$ m below the summit; thus, $z \simeq 725$ m). Further investigation is needed regarding the different origin of these structures.

4.3. Influence of the Hydrodynamics on CWC Ecosystem Functioning

While the size of the CWC mounds has been shown to play a role in the hydraulic control of the flow over them, questions are raised regarding the influence of hydrodynamics on CWC ecosystem functioning and reef and mound growth. Recent video footage by our team (unpublished results) suggests that while healthy corals are found at the summit of smaller mounds, they are virtually absent from the summit of bigger mounds (although found on their flanks; see *van Bleijswijk et al.* [2015]). This may suggest that the Haas mound has reached its maximum height while the smaller mound still grows vertically. This observation may be counterintuitive since it is generally accepted that dynamical environments (strong currents and mixing zones) such as over the top of Haas mound are favorable for CWC [e.g., *Genin et al.*, 1986; *Frederiksen et al.*, 1992; *Roberts et al.*, 2006; *Davies et al.*, 2009; *White and Dorschel*, 2010]. In other words, a challenging question for CWC ecosystem functioning and reef and mound development on the slopes of Rockall Bank is raised: *How does mound size influence the hydrodynamics, and vice versa?* This work partly answers this question by suggesting that by modifying the hydrodynamics, CWC mounds maintain, up to a certain extent, a turbulent environment favorable for their growth. However, by outgrowing themselves they significantly block the flow ($Fr < 1$) and prevent the deep nutrient-rich water to periodically wash their summit. Then, these mounds may reach a steady state where they can no longer grow vertically in their actual physical and biogeochemical environment. Environmental parameters driving this maximum height may be different from one region to another, since they depend on the barotropic tidal flow and on the vertical distribution of nutrients. More field work is, however, needed to verify this hypothesis, which should include physiological and geochemical tracers measurements above these mounds and geological analyses of CWC mound growth rates.

Acknowledgments
The authors would like to thank the captain and crew of the R/V *Pelagia*. F. Cyr would like to thank R. Chassagne, A. Cimatoribus, L. Maas, and H. Malschaert for their help. F. Mienis was funded by the Innovational Research Incentives Scheme of the Netherlands Organization for Scientific Research (NWO VENI) and F. Cyr by the Fonds de recherche du Québec - Nature et technologies (FRQNT) postdoctoral fellowship program. D. Bourgault is a member of the strategic network Québec-Océan.

References

Bourgault, D., and D. E. Kelley (2004), A laterally averaged nonhydrostatic ocean model, *J. Atmos. Oceanic Technol.*, *21*, 1910–1924.
Bourgault, D., M. Morsilli, C. Richards, U. Neumeier, and D. Kelley (2014), Sediment resuspension and nepheloid layers induced by long internal solitary waves shoaling orthogonally on uniform slopes, *Cont. Shelf Res.*, *72*, 21–33, doi:10.1016/j.csr.2013.10.019.
Cartwright, D. E. (1969), Extraordinary tidal currents near St Kilda, *Nature*, *223*, 928–932.
Cyr, F., and H. van Haren (2015), Observations of small-scale secondary instabilities during the shoaling of internal bores on a deep-ocean slope, *J. Phys. Oceanogr.*, *46*, 219–231, doi:10.1175/JPO-D-15-0059.1.
Davies, A., G. Duineveld, M. Lavaleye, M. Bergman, H. van Haren, and J. Roberts (2009), Downwelling and deep-water bottom currents as food supply mechanisms to the cold-water coral Lophelia pertusa (Scleractinia) at the Mingulay Reef complex, *Limnol. Oceanogr.*, *54*(2), 620–629, doi:10.4319/lo.2009.54.2.0620.
Duineveld, G. C. A., M. S. S. Lavaleye, M. J. N. Bergman, H. De Stigter, and F. Mienis (2007), Trophic structure of a cold-water coral mound community (Rockall Bank, NE Atlantic) in relation to the near-bottom particle supply and current regime, *Bull. Mar. Sci.*, *81*(3), 449–467.
Findlay, H. S., S. J. Hennige, L. C. Wicks, J. M. Navas, E. M. S. Woodward, and J. M. Roberts (2014), Fine-scale nutrient and carbonate system dynamics around cold-water coral reefs in the northeast Atlantic, *Sci. Rep.*, *4*, 3671, doi:10.1038/srep03671.
Frederiksen, R., A. Jenssen, and H. Westerberg (1992), The distribution of the scleractinian coral Lophelia pertusa around the Faeroe Islands and the relation to internal tidal mixing, *Sarsia*, *77*, 157–171.
Genin, A., P. K. Dayton, P. F. Lonsdale, and F. N. Spiess (1986), Corals on seamount peaks provide evidence of current acceleration over deep-sea topography, *Nature*, *322*(6074), 59–61, doi:10.1038/322059a0.
Henry, L. A., and J. M. Roberts (2007), Biodiversity and ecological composition of macrobenthos on cold-water coral mounds and adjacent off-mound habitat in the bathyal Porcupine Seabight, NE Atlantic, *Deep Sea Res., Part I*, *54*(4), 654–672, doi:10.1016/j.dsr.2007.01.005.
Henry, L. A., J. Moreno Navas, and J. M. Roberts (2013), Multi-scale interactions between local hydrography, seabed topography, and community assembly on cold-water coral reefs, *Biogeosciences*, *10*(4), 2737–2746, doi:10.5194/bg-10-2737-2013.
Huthnance, J. (1974), On the diurnal tidal currents over Rockall Bank, *Deep Sea Res. Oceanogr. Abstr.*, *21*(1), 23–35, doi:10.1016/0011-7471(74)90016-3.
Klymak, J. M., S. Legg, and R. Pinkel (2010), A simple parameterization of turbulent tidal mixing near supercritical topography, *J. Phys. Oceanogr.*, *40*(9), 2059–2074, doi:10.1175/2010JPO4396.1.
Legg, S., and J. M. Klymak (2008), Internal hydraulic jumps and overturning generated by tidal flow over a tall steep ridge, *J. Phys. Oceanogr.*, *38*(9), 1949–1964, doi:10.1175/2008JPO3777.1.
Longuet-Higgins, M. S. (1968), Double Kelvin waves with continuous depth profiles, *J. Fluid Mech.*, *34*(01), 49–80, doi:10.1017/S002211206800176X.
McGrath, T., G. Nolan, and E. McGovern (2012), Chemical characteristics of water masses in the Rockall Trough, *Deep Sea Res., Part I*, *61*, 57–73, doi:10.1016/j.dsr.2011.11.007.
Mienis, F., T. van Weering, H. de Haas, H. de Stigter, V. Huvenne, and a. Wheeler (2006), Carbonate mound development at the SW Rockall Trough margin based on high resolution TOBI and seismic recording, *Mar. Geol.*, *233*(1–4), 1–19, doi:10.1016/j.margeo.2006.08.003.
Mienis, F., H. C. de Stigter, M. White, G. Duineveld, H. de Haas, and T. C. E. van Weering (2007), Hydrodynamic controls on cold-water coral growth and carbonate-mound development at the SW and SE Rockall Trough Margin, NE Atlantic Ocean, *Deep Sea Res., Part I*, *54*(9), 1655–1674, doi:10.1016/j.dsr.2007.05.013.
Mohn, C., A. Rengstorf, M. White, G. Duineveld, F. Mienis, K. Soetaert, and A. Grehan (2014), Linking benthic hydrodynamics and cold-water coral occurrences: A high-resolution model study at three cold-water coral provinces in the NE Atlantic, *Prog. Oceanogr.*, *122*, 92–104, doi:10.1016/j.pocean.2013.12.003.
Moray, R. (1665), A relation of some extraordinary tydes in the West-Isles of Scotland, as it was communicated by Sr. Robert Moray, *Philos. Trans.*, *1*, 53–55.
Moreno Navas, J., P. L. Miller, L. A. Henry, S. J. Hennige, and J. M. Roberts (2014), Ecohydrodynamics of cold-water coral reefs: A case study of the Mingulay Reef Complex (Western Scotland), *PLoS One*, *9*(5), 1–12, doi:10.1371/journal.pone.0098218.
Pingree, R. D., and D. K. Griffiths (1984), Trapped diurnal waves on Porcupine and Rockall Banks, *J. Mar. Biol. Assoc. U. K.*, *64*, 889–897.
Roberts, J. M., A. J. Wheeler, and A. Freiwald (2006), Reefs of the deep: The biology and geology of cold-water coral ecosystems, *Science*, *312*(5773), 543–547, doi:10.1126/science.1119861.
Roberts, J. M., L. a. Henry, D. Long, and J. P. Hartley (2008), Cold-water coral reef frameworks, megafaunal communities and evidence for coral carbonate mounds on the Hatton Bank, North East Atlantic, *Facies*, *54*(3), 297–316, doi:10.1007/s10347-008-0140-x.
Rüggeberg, A., S. Flögel, W. C. Dullo, K. Hissmann, and A. Freiwald (2011), Water mass characteristics and sill dynamics in a subpolar cold-water coral reef setting at Stjernsund, northern Norway, *Marine Geology*, *282*(1–2), 5–12, doi:10.1016/j.margeo.2010.05.009.
Smagorinsky, J. (1963), General circulation experiments with the primitive equations, *Mon. Weather Rev.*, *91*(3), 99–164, doi:10.1126/science.27.693.594.
Thierens, M., J. Titschack, B. Dorschel, V. a. I. Huvenne, a. J. Wheeler, J. B. Stuut, and R. O'Donnell (2010), The 2.6 Ma depositional sequence from the Challenger cold-water coral carbonate mound (IODP Exp. 307): Sediment contributors and hydrodynamic palaeo-environments, *Mar. Geol.*, *271*(3–4), 260–277, doi:10.1016/j.margeo.2010.02.021.
van Bleijswijk, J. D. L., C. Whalen, G. C. A. Duineveld, M. S. S. Lavaleye, H. J. Witte, and F. Mienis (2015), Microbial assemblages on a cold-water coral mound at the SE Rockall Bank (NE Atlantic): Interactions with hydrography and topography, *Biogeosciences*, *12*(14), 4483–4496, doi:10.5194/bg-12-4483-2015.
van Haren, H., F. Mienis, G. C. A. Duineveld, and M. S. S. Lavaleye (2014), High-resolution temperature observations of a trapped nonlinear diurnal tide influencing cold-water corals on the Logachev mounds, *Prog. Oceanogr.*, *125*, 16–25, doi:10.1016/j.pocean.2014.04.021.
White, M., C. Mohn, H. de Stigter, and G. Mottram (2005), Deep-water coral development as a function of hydrodynamics and surface productivity around the submarine banks of the Rockall Trough, NE Atlantic, in *Cold-water Corals and Ecosystems*, pp. 503–514, Springer, Berlin.
White, M., and B. Dorschel (2010), The importance of the permanent thermocline to the cold water coral carbonate mound distribution in the NE Atlantic, *Earth Planet. Sci. Lett.*, *296*(3–4), 395–402, doi:10.1016/j.epsl.2010.05.025.
White, M., J. M. Roberts, and T. Weering (2007), Do bottom-intensified diurnal tidal currents shape the alignment of carbonate mounds in the NE Atlantic?, *Geo-Mar. Lett.*, *27*(6), 391–397, doi:10.1007/s00367-007-0060-8.